International Journal of Scientific Engineering and Technology
Volume No.5 Issue No.12, pp: 549-555

ISSN:2277-1581
01 December 2016

Characterization of Steam Oxide Morphology for Advanced Heat Resistant Steel

Hafizzudin B. Kasim[1], Firas B. Ismail Alnaimi1[2]
[1]TNB Research Sdn Bhd [2]Power Generation Research Centre, College of Engineering, Universiti Tenaga Nasional (UNITEN),
Putrajaya Campus, Jalan IKRAM-UNITEN, 43000 Kajang, Selangor, Malaysia

Abstract : Supercritical power plants have now become one of the essential plans for the power generation industry due its higher efficiency and larger capacity compare to the current power plant in Malaysia. To increase the confidence level in plant assessment, a study have been initiated to study the steam oxide morphology in supercritical boiler technology. The data captured will be used as baseline and reference data for boiler tube wall assessment.

Keywords: Oxide morphology, supercritical power plant

1.0 Introduction

For a boiler tubes within a power plant, there are basically have two factors that govern the life of boiler tubes which is creep mechanism and also steam oxidation. The current condition assessment of boiler tube monitoring for Risk Based Inspection (RBI) in Tenaga Nasional Berhad (also known as TNB, utility power in Malaysia) plants were only depends on trending and minimum acceptable tube thickness limits supply from the manufacturer. There are no references or acceptance criteria for wall thinning rate caused by steam oxidation. Hence, study on steam oxidation behavior at specific material used in TNB power plants are essential to increase the confidence level in boiler tube condition assessment. Steam oxide scale were highly dependent on metallurgical type of material used, time and temperature exposed onto boiler tube.

2.0 Methodology

Phase	Description
Phase 1	Selection of material (T91, T92, TP 347 H and Super 304 H).
Phase 2	Autoclave simulation at specified temperature & pressure.
Phase 3	Withdraw the tube samples at predetermined time interval.
Phase 4	Examine the oxide growth and alloy using conventional & advanced metallographic testing facilities. (SEM / Optical Microscope / Mirovickers hardness testing).

2.1 Phase 1 - Selection of material

Four different type of material had been selected which are T91, T92, TP 347 H and Super 304 H. The selection of material is based from actual material used in current boiler and future supercritical boiler technology. T91 and T92 were supplied from the actual test tube sample by TNB while TP 347 H and Super 304 H were supplied by KEPRI (power utility in Korea). These four different type of materials are also choose based on their ferritic and austenitic steel characteristics. Material T91 and T92 were both ferritic steel while the other two steel, TP 347 H and Super 304 H were austenitic steel

2.2 Phase 2 - Autoclave simulation

Once the sample had been acquired, these samples will be sent to KEPRI's laboratory to be put into steam autoclaves The purpose of steam auto clave is to simulate the dry steam condition in supercritical boiler. The autoclave will apply specific pressure and heat as specified by operator. The pressurized steam is circulated through the tubes giving the actual condition of tubes exposure. Test temperatures are 600℃, 650℃ and 700℃ for 25,000 hours under steam environment. Sampling interval is 2,500hrs, 5,000hrs, 10,000hrs, 15,000hrs, 20,000hrs and 25,000hrs.

2.3 Phase 3 - Withdraw the tube samples at predetermined time interval

Throughout the experimental period, sample from exposure hour 2500 hour and 5000 hour will be extracted out from autoclave for further steam oxide morphology analysis. In the actual full research, the sample will further continue up until 20,000 exposure hour, but for this research study, it will be limited to 5000 exposure hour. The reason these time interval were selected is for a comprehensive study can be made to the oxidation growth in stage of 2500 hour exposure interval. The existing publishes data mainly on short term experiments and at accelerated condition in which the samples were conditioned in steam autoclaves with higher temperature and shorter conditioning time. Therefore, factor of exfoliation may not be accounted in these existing studies. But, as for this study, the scope of research will focus on lower temperature close to design temperature with longer conditioning time, thus, oxidation characteristics will be more representative to the actual profile in the boilers and the data can be used as references to TNB.

2.4 Phase 4 - Examine the oxide growth and alloy using conventional & advanced metallographic

ISSN:2277-1581
01 December 2016

By the time the tube samples were being withdrawn out at predetermined time interval, the tubes were cut in longitudinal section and mounted using cold mounting technique. The mounted specimens were ground and polished and then etched to reveal the microstructure. Further morphological analysis the oxide growth and base alloy will be examine by using conventional and advanced metallographic testing facilities in material testing laboratory in TNBR. The equipment used includes Hitachi S8000 Scanning Electron Microscope (SEM) equipped with Electron Dispersive X-ray (EDX), conventional optical microscope and Microvicker hardness testing. For conventional optical microscope, the microstructure examination will be carried out up to magnification of 500 times. For Microvicker hardness testing, the hardness testing was performed on the etched, mounted specimens with the test load 300 gf, indented for 15 seconds with five indentations were made on each of tube samples.

2.4.1 SEM / EDX Working Principle

In general, Scanning electron microscope (SEM) and Energy – Dispersive X-Ray Spectroscopy (EDX) is an analytical technique used for the elemental analysis or chemical characterization of a specific sample. At the first stage, through field emission process by electron gun, beam of electron is being generated and it's being accelerated through the high voltage produce by anode ring. This high voltage basically can be varied from 2 kV up until 20 kV, depending on different type of sample used. For this project, the voltage applied is 15 kV. These highly accelerated electrons will pass through the electromagnetic lenses to produce a thin beam of electrons, passing through the scanning oil. Within the scanning coil, the specimen will be scanned simultaneously while the thin electron beam will hit the specimen, causing different wavelength electrons emitted from the specimen. Noted that, different type of element composition, will produced different type of wavelength, and these variations of electron's wavelength will be collected by the suitable detector to produce spectrum as shown in the screen monitor.

2.4.2 Optical Microscope Working Principle

Optical microscope is a device that used to magnify images for small samples. The source of light used is visible light from bulb install within the device. The magnification of images may be range from 50x magnification to 5000x magnification from actual size. The optical microscope used in this research is able to capture digital magnified images through charge-coupled devices (CCD) cameras installed in the device. For this research project, compound microscope is used. The compound microscope has two lenses which are eyepiece lens and objective lens. The objective lens will focus on sample with built-in light, and then project the images to eyepiece lens. From here, the images will be magnified and ready to be captured by CCD cameras. The images magnifications applied to observe the oxidation growth are 50x, 100x, 200x and 500x times magnification.

2.4.3 Microvickers hardness test working principle

Hardness is generally a unit of measurement in mechanical properties to resist the plastic deformation region. Hardness value may be varies according to material-alloy specification, material degradation and material current conditions. For this research project, considering the sample being executed in autoclave simulation and exposed to high temperature, the establishment of hardness pattern is important to verify the presences of material degradation within the sample. The proposed and available testing methods is microvicker hardness testing.

Microvickers hardness testing is a method consists of indentation of diamond indenter into the sample and hardness value for the material is able to be calculated. The load applied onto diamond indenter is subject to type of material tested. The available load are varies from 1 kgf to 1000 kgf. The indention time also depending on type of material tested. The time may varies from 5 seconds to 30 seconds. Considering the sample studied is austenitic and ferritic steel which are by literature review show intermediate hardness values, the proposed load and time of indention is 300 kgf for 15 seconds.

Once the sample is subject to indentation procedure, the diamond indenter will left two diagonal surfaces on samples. The average perimeter of this diamond-shape will be calculated and the results will be compared to Vickers standard for actual hardness value. Five reading were taken across the sample thickness. The locations of indentation are as Figure 3.3 below:

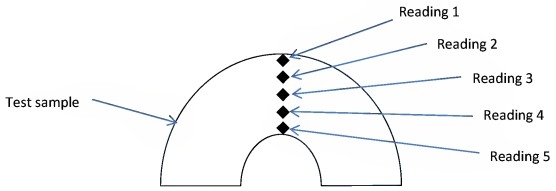

Figure 3.3: The location of hardness indentation

3.0 Results and Discussion

Literature reviews on steam oxidation behavior were referred to several of author [1 - 30]. In this chapter, the results of laboratory examination will be presented and further discussed. The oxide scale and characteristics for each tested material will compared and tabulated. The pattern of oxide thickness and hardness will be established by plotted graph.

Material : T91	
Exposure Temperature: 600^{o}C	
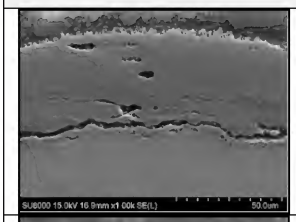	Exposure Hour : 2500 hour Oxide Thickness : 45 µm
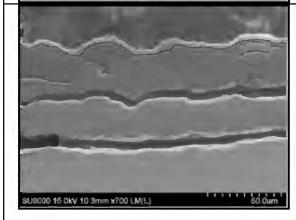	Exposure Hour : 5000 hour Oxide Thickness: 59.28 µm
Exposure Temperature: 650^{o}C	

ISSN:2277-1581
01 December 2016

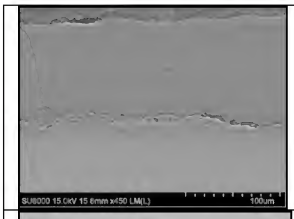	Exposure Hour : 2500 hour Oxide Thickness: 96.32 µm
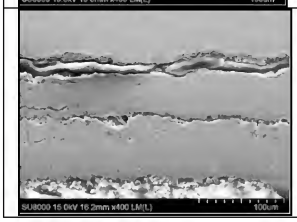	Exposure Hour : 5000 hour Oxide Thickness: 127.5 µm

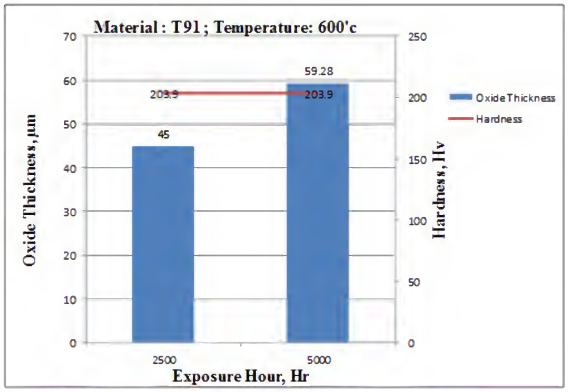

Graph 3.1 : The comparison graph for material T91 at temperature of 600°C between exposure hour of 2500 hour and 5000 hour.

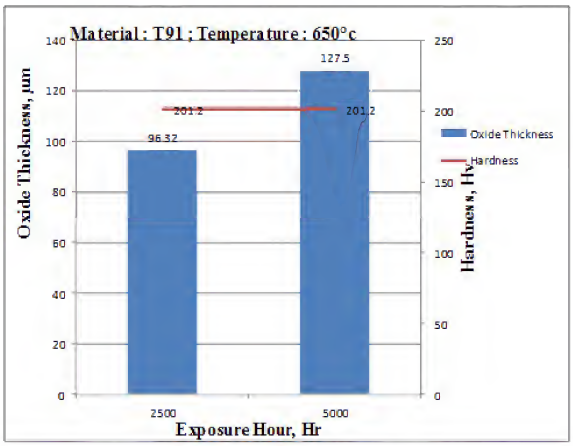

Graph 3.2 : The comparison graph for material T91 at temperature of 650°C between exposure hour of 2500 hour and 5000 hour.

Material : T92	
Exposure Temperature: 600°C	
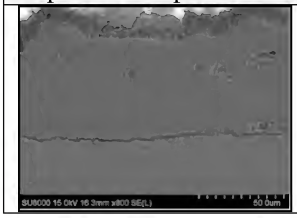	Exposure Hour: 2500 hour Oxide Thickness: 48.02 µm

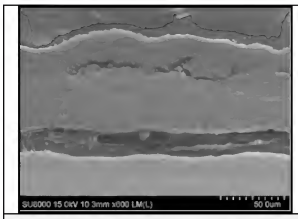	Exposure Hour : 5000 hour Oxide Thickness: 65.76 µm
Exposure Temperature: 650°C	
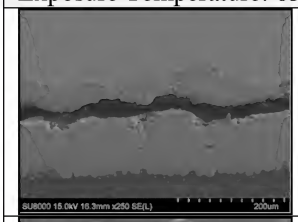	Exposure Hour: 2500 hour Oxide Thickness: 95.26 µm
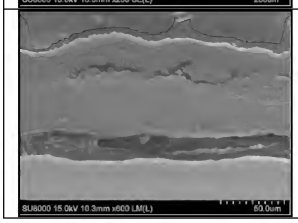	Exposure Hour: 5000 hour Oxide Thickness: 141.9 µm

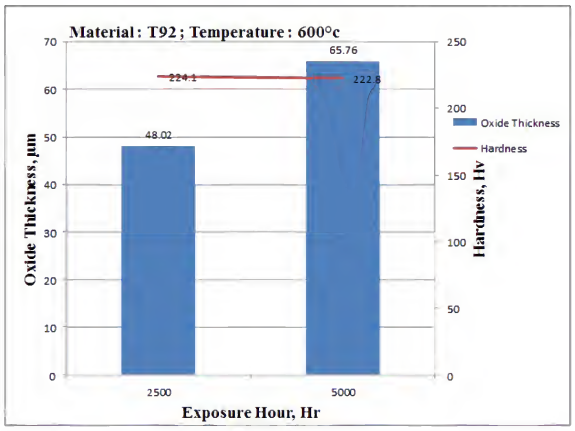

Graph 3.3 : The comparison graph for material T92 at temperature of 600°C between exposure hour of 2500 hour and 5000 hour.

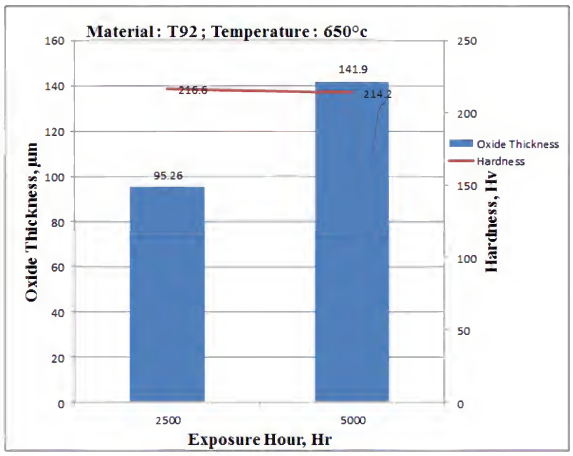

Graph 3.4 : The comparison graph for material T92 at temperature of 650°C between exposure hour of 2500 hour and 5000 hour.

doi : 10.17950/ijset/v5s12/1206

ISSN:2277-1581
01 December 2016

Material : T 304 H	
Exposure Temperature: 600°C	
	Exposure Hour: 2500 hour Oxide Thickness: 10.52 µm
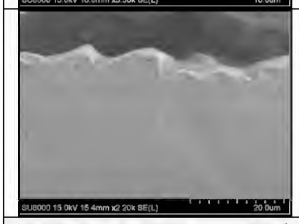	Exposure Hour: 5000 hour Oxide Thickness: 8.9 µm
Exposure Temperature: 650°C	
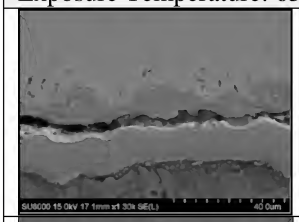	Exposure Hour: 2500 hour Oxide Thickness: 28.3 µm
	Exposure Hour : 5000 hour Oxide Thickness: 24.86 µm

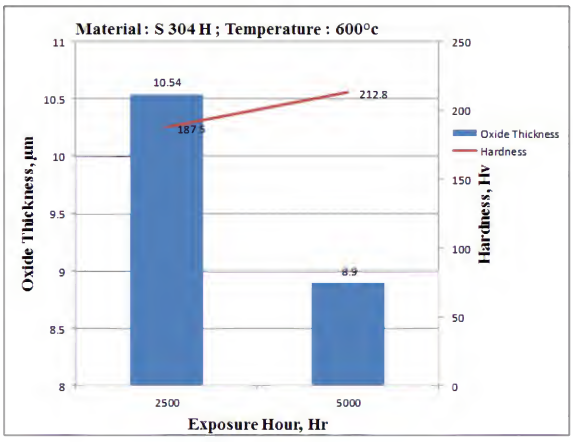

Graph 3.5 : The comparison graph for material S304H at temperature of 600°C between exposure hour of 2500 hour and 5000 hour. The average hardness and oxidation thickness were increased.

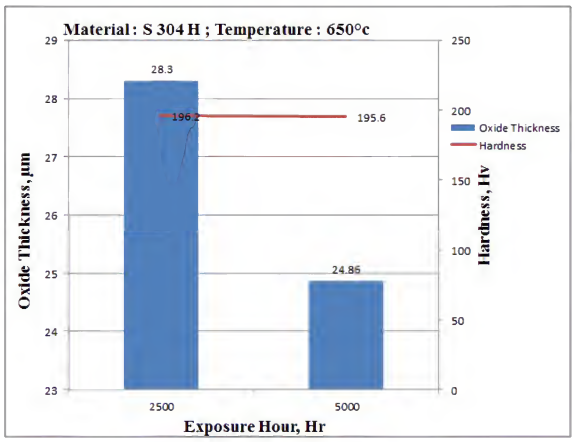

Graph 3.6 : The comparison graph for material S304H at temperature of 650°C between exposure hour of 2500 hour and 5000 hour. The average hardness were almost identical, while oxidation thickness were decreased.

Material : T 347 H	
Exposure Temperature: 600°C	
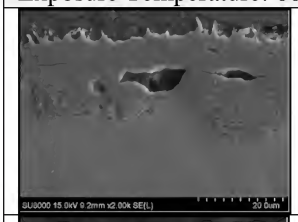	Exposure Hour: 2500 hour Oxide Thickness: 19.3 µm
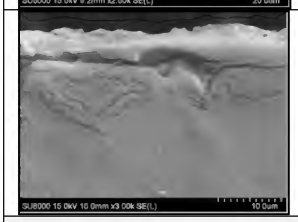	Exposure Hour : 5000 hour Oxide Thickness: 10.66 µm
Exposure Temperature: 650°C	
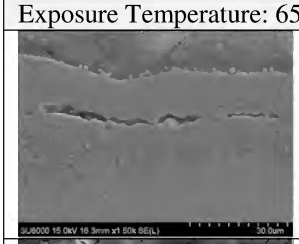	Exposure Hour: 2500 hour Oxide Thickness: 46.4 µm
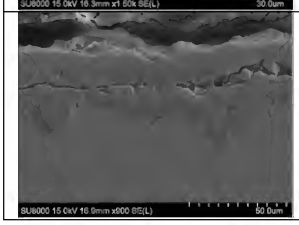	Exposure Hour: 5000 hour Oxide Thickness: 22.7 µm

International Journal of Scientific Engineering and Technology
Volume No.5 Issue No.12, pp: 549-555
ISSN:2277-1581
01 December 2016

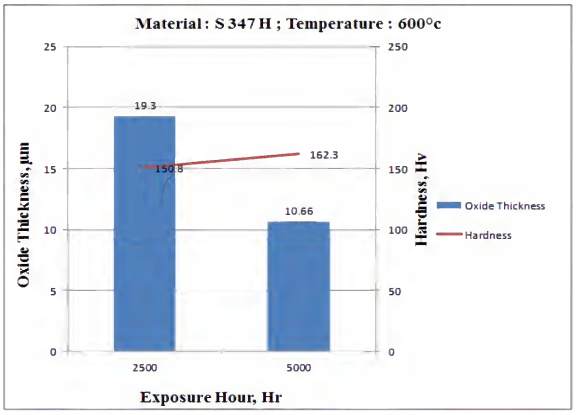

Graph 3.7 : The comparison graph for material S347H at temperature of 650°C between exposure hour of 2500 hour and 5000 hour. The average hardness were increased, while oxidation thickness were decreased.

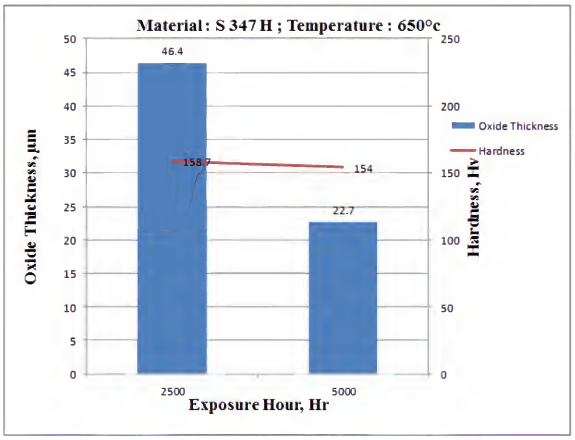

Graph 3.8 : The comparison graph for material T91 at temperature of 650°C between exposure hour of 2500 hour and 5000 hour. The average hardness were almost identical, while oxidation thickness were decreased.

3.1 Oxidation growth rate

The results above and steam oxidation rate were summarized as below:

Thickness Value (µm)			Oxidation Growth Rate (µm) / 1000 hrs	
Exposure Hour : 0000 hr	Exposure Hour : 2500 hr	Exposure Hour : 5000 hr	0000 hr - 2500 hr	2500 hr - 5000 hr
Material : T91				
Temperature Exposed : 600^{0}c				
0	45	59.28	18	5.712
Temperature Exposed : 650^{0}c				
0	96.32	127.5	38.528	12.47
Material : T92				
Temperature Exposed : 600^{0}c				
0	48.02	65.76	19.208	7.096
Temperature Exposed : 650^{0}c				
0	95.26	141.9	38.104	18.66
Material : S 304 H				
Temperature Exposed : 600^{0}c				
0	10.54	8.9	4.216	-0.656
Temperature Exposed : 650^{0}c				
0	28.3	24.86	11.32	-1.376
Material : 347 H				
Temperature Exposed : 600^{0}c				
0	19.3	10.66	7.72	-3.456
Temperature Exposed : 650^{0}c				
0	46.4	22.7	18.56	-9.48

Table 3.1: The comparison between oxidation growth rate at interval of 2500 hr.

The oxidation growth rate for each material at different temperature and exposure hour were tabulated. For exposure hour between 0000 hrs and 2500 hour, the highest oxidation growth rate was recorded by material T91 at 650^{0}C with value of 38.528 µm / 1000 hrs. Meanwhile, the lowest oxidation growth rate was recorded by material S 304 H at 600^{0}C with value of 4.216 µm / 1000 hrs.

For exposure hour between 2500 hour and 5000 hour, the highest oxidation growth rate was recorded by material T92 at 650^{0}C with value of 18.656 µm / 1000 hrs. The lowest oxidation growth rate was recorded by material S 304 H at 600^{0}C with value of 0.656 µm / 1000 hrs.

3.2 Mechanism of Oxide Growth

The element such as molybdenum and chromium that contained in ferritic steel are known for its resistance in most of damage found in thermal power plants, such as creep damage, thermal fatigue, carbonization, corrosion and others. For austenitic steel, its mechanical properties may offered higher stress resistance at higher temperature compared to ferritic steel. [34]. Depending on the type of equipment, both of steel may be utilized based upon their characterisation. In this study, steam oxidation morphology for both material were further discussed and compared. For all condition, the hematite formation were observed as an outermost oxidation layer. This is due to instability of magnetite thermodynamic properties which react with steam (high oxygen potential). The chemical reaction as such were establisehed [35]:

$2Fe_3O_4 + H_20 \rightarrow 3Fe_2O_3 + H_2$ (3.1)

The prolonged exposure of oxidation may also decrease the heat transfer rate to the medium and boiler tube. This may lead short term overheating and degradation of tube alloy, thus causing boiler tube failures. Statistically, 10% off all plant breakdown was due to creep fractures of boiler tubes due to accumulated scale formation. [36]

For ferritic material (T91 and T92), the oxide thickness in averagehad had increased between 2500 exposure hour to 5000 exposure hour. From optical microscope images, the oxide layer for these material had not undergone spallation process yet, explaining the increased value of thickness. For hardness reading, the values did not have much variation between 2500 exposure hour to 5000 exposure hour.

As for austenitic steel (T304H and T347H), the oxide thickness in averaged had decreased between 2500 exposure hour and 5000 exposure hour. Unlike ferritic steel, the spallation process had been undergone in austenitic steel from the oprtical microsocope images. For hardness reading, the values also did

ISSN:2277-1581
01 December 2016

not have signifance variation between 2500 exosure hour to 5000 exposure hour.

The ferritic 9-12% Cr steel, the oxidation rates tends to be very low especially within its incubation period during simulation in autoclave compared to austenitic steel. This incubation period is depending on amount of protective layers and types of cold work applied where it may vary from minutes to hundreds of hours.

Based on EDX results as shown in Figure 4.2 – 4.16, the oxidation layers formed were consisting of Cr-rich $(Fe,Cr)_3O_4$ or $(Fe,Cr)_2O_3$. These oxidation layer breakdowns were normally related to the growth of magnetite or hematite layer which build up from Cr_2O_3 precipitates within FeO matrix. The gap observed between inner and outer layer of were caused by rapid growth of outer magnetite layer, hence resulting a phenomenon called vacancy condensation. This gap serves as a bridge for ion transportation process such as Fe, O and others. As the overall oxide layer thickness is increasing, the gap between inner and outer layer will also be increase, thus the rate of ion transfer activity will be reduced due to difficulty. Haematite layer will be formed on top of the scale due to this decreasing of ion activity

The spallation of oxide scales in water vapour were always associated with numbers of defects such as microvoids, voids or pores presence that eventually created a gap between oxide scales and base metal. Based on the literature review, these defects were resulted from ion migration, thus promoted vacancy coagulation. For multi layered oxide scales (such as haematite and magnetite layer), the voids were also promoted by the interferences of these oxide phase. [37]

Based on oxide morphology structures exhibit for each material tested, it have the important factors that control the oxidation rate. The outer most layer was formed through chemical reaction with steam water at contact surface and created magnetite layer with columnar grains. This magnetite layer was consisted of high porosity structure, thus its diffusivity characteristics became more effective. For inner layer, the structures were denser as compared to outer layer and serve as protective oxide film for the base metal of an alloy. These inner oxide were generated from inward diffusions of oxygen to the oxide metal surface [38,39]

4.0 Conclusions

Study of oxidation growth behavior on material T91, T92, S304H and S3047 were carried out. The material were being exposed to temperature of 600^0C and 650^oC, while exposed time are 2500 hour and 5000 hour. From the pattern showed above, it was observed the highest oxidation growth rates were occurring at higher temperature exposed. This observation is applicable to each material at all exposure hour. Another observation shows the oxidation growth rate had increased rapidly between the exposure hour of 0000 hrs and 2500 hrs as compared to exposure hour of 2500 hrs and 5000 hrs.

The rapid spallation of oxide layer may cause blockage, hence reducing heat transfer rate from flue gas to steam within boiler tube. The reduced heat transfer rate may cause low efficiency of power plant output and also overheat the boiler tubes specifically at blockage area. For overheated boiler tube, the material will slowly degrade overtime and mechanical properties such as hardness value will also change. This symptom is commonly known as failure root cause of boiler tubes.

From the results of oxidation growth rate, power plant station shall pay more attention during their overhaul period to carry out a proper oxide cleaning at boiler tubes which exposed to higher temperature. This may avoid unnecessary tube failure incident and extra cost of repairing.

4.1 References

i. *Alina Agüero a,*, Vanessa González a, Peter Mayr b, Krystina Spiradek-Hahn c, Anomalous steam oxidation behavior of a creep resistant martensitic 9 wt. % Cr steel, Materials Chemistry and Physics 141 (2013) 432e439.*

ii. *D.R.H Jones, Creep failures of overheated boiler, superheater and reformer tubes, Engineering Failure Analysis, Volume 11, Issue 6, December 2004, Pages 873–893*

iii. *P. Mayer, A.V. Manolescu, Oxidation of boiler tube steels in steam, Proceedings of Metallurgical Society of Canadian Institute of Mining and Metallurgy, 1990, Pages 276–295*

iv. *Zs. To¨kei, H. Viefhaus, H.J. Grabke, Initial stages of oxidation of a 9CrMoV-steel: role of segregation and martensite laths, Applied Surface Science 165 _2000. 23–33*

v. *http://www.outokumpu.com/en/stainless-steel/grades/heat-resistant/Pages/default.aspx*

vi. *http://www.larsentoubro.com/lntcorporate/common/ui_templates/HtmlContainer.aspx?res=P_PWR_DSCT*

vii. *G. von Heiermann et al, Dampferzeuger für fortgeschrittene Dampfparameter. VGB Kraftwerkstechnik 73 (1993). H. 8. S. 678-689.*

viii. *S.R.J. Saunders, M. Monteiro, F. Rizzo, The oxidation behaviour of metals and alloys at high temperatures in atmospheres containing water vapour: a review, Progress in Materials Science 53 (2008) 775–837.*

ix. *W.J. Quadakkers, J. Z_urek, M. Hänsel, Effect of water vapor on hight emperature oxidation of FeCr alloys, JOM Journal of the Minerals Metals and Materials Society 61 (2009) 44–50.*

x. *G.S. Was, S. Teysseyre, J. McKinley, in: Proceeding of Corrosion 2004, NACE International, 2004, Paper 04492.*

xi. *J.C. Nava Paz, R. Knödler, Materials for Advanced Power Engineering (1998) 451.*

xii. *R. Knödler, B. Scarlin, Materials for Advanced Power Engineering (2002) 1601.*

xiii. *J. Zurek, L. Nieto-Hierro, J. Piron-Abellan, L. Niewolak, L. Singheiser, W.J. Quadakkers, Materials Science Forum 461e464 (2004) 791.*

xiv. *Mingcheng Sun, Xinqiang Wu, Zhaoen Zhang, En-Hou Han, Analyses of oxide films grown on Alloy 625 in oxidizing supercritical water, Journal of Supercritical Fluids 47 (2008), Page 309–317*

xv. *Alina Agüero, Vanessa González, Peter Mayr, Krystina Spiradek-Hahn, Anomalous steam oxidation behavior of a creep resistant martensitic 9 wt. % Cr steel, Materials Chemistry and Physics 141 (2013), Page 432 - 439*

xvi. *J.Zurek, E. Wessel, L. Niewolak, F. Schmitz,T.-U. Kern, L. Singheiser, W.J. Quadakkers, Anomalous temperature dependence of oxidation kinetics during steam oxidation of ferritic steels in the temperature range 550–650 ^{o}C, Corrosion Science 46 (2004), Page 2301–2317*

xvii. *Xin Gao, Xinqiang Wu, Zhaoen Zhang, Hui Guan, En-hou Han, Characterization of oxide films grown on 316L stainless steel exposed to H2O2-containing supercritical water, Journal of Supercritical Fluids 42 (2007) Page 157–163*

ISSN:2277-1581
01 December 2016

xviii. *Dionisio Laverde, Tomas Goomez-Acebo, Francisco Castro, Continuous and cyclic oxidation of T91 ferritic steel under steam, Corrosion Science 46 (2004) Page 613–631*

xix. *Yongsun Yi, Byeonghak Lee, Sungho Kim, Jinsung Jang, Corrosion and corrosion fatigue behaviors of 9cr steel in a supercritical water condition, Materials Science and Engineering A 429 (2006) Page 161–168*

xx. *L. Tan, X. Ren, T.R. Allen, Corrosion behavior of 9–12% Cr ferritic–martensitic steels in supercritical water, Corrosion Science 52 (2010) Page 1520–1528*

xxi. *J. M. Sarver, Charactrization of Steam-Formed Oxides on Candidate Materials for USC Boilers, Advanced in Material Technology for Fossil Power Plants Proceedings from the Sixth International Conference, 2012, Pages 198 – 211*

xxii. *Adrian S. Sabau, John P. Shingledecker and Ian G. Wright, Steam-Side Oxide Scale Exfoliation Behaviour in Superheater and Reheaters: Differences in the Behavior of Alloys T22, T91 and T347 Based on Computer Simulation Results, Advanced in Material Technology for Fossil Power Plants Proceedings from the Sixth International Conference, 2010, Pages 213-242*

xxiii. *A Fry, S Osgerby, M Wright, Oxidation of Alloys in Steam Environments – A Review, NPL Report MATC (A) 90, September 2002, Pages 1-49.*

xxiv. *Kaiju Yin, Shaoyu Qiu, Rui Tang, Qiang Zhang, Lefu Zhang, Corrosion behavior of ferritic/martensitic steel P92 in supercritical water, Journal of Supercritical Fluids 50 (2009), Page 235–239*

xxv. *Yun Chen, Kumar Sridharan, Todd Allen, Corrosion behavior of ferritic - martensitic steel T91 in supercritical water, Corrosion Science 48 (2006) 2843–2854*

xxvi. *Jeremy Bischoff, Arthur T. Motta, Chad Eichfeld, Robert J. Comstock, Guoping Cao, Todd R. Allen, Corrosion of ferritic–martensitic steels in steam and supercritical water, Journal of Nuclear Materials 441 (2013) Page 604–611*

xxvii. *J. Ehlers, D.J. Young, E.J. Smaardijk, A.K. Tyagi, Enhanced oxidation of the 9%Cr steel P91 in water vapour containing environments, Corrosion Science 48 (2006), Page 3428–3454*

xxviii. *P.J. Ennis, W.J. Quadakkers, Implications of steam oxidation for the service life of high-strength martensitic steel components in high-temperature plant, International Journal of Pressure Vessels and Piping 84 (2007), Page 82–8*

xxix. *I. Iordanova, K.S. Forcey, R. Harizanova , Y. Georgiev, M. Surtchev, Investigation of structure and composition of surface oxides in a high chromium martensitic steel, Journal of Nuclear Materials 257 (1998) Page 126-133*

xxx. *P.J. Ennis, W.J. Quadakkers, Mechanisms of steam oxidation in high strength martensitic steels, International Journal of Pressure Vessels and Piping 84 (2007) Page 75–81*

xxxi. *Yun Chen, Kumar Sridharan, Todd R. Allen, Shigeharu Ukai, Microstructural examination of oxide layers formed on an oxide dispersion strengthened ferritic steel exposed to supercritical water, Journal of Nuclear Materials 359 (2006) Page 50–58*

xxxii. *M. Halvarssona,, J.E. Tang, H. Asteman, Microstructural investigation of the breakdown of the protective oxide scale on a 304 steel in the presence of oxygen and water vapour at 600 ^{o}C, Corrosion Science 48 (2006) Page 2014–2035*

xxxiii. *J. Zurek, L. Nieto-Hierro, P.J. Ennis, L. Singheiser and W.J. Quadakkers, Oxidation behavior of ferritic and austenitic steels in simulated steam environments, Proceeding from the fourth international conferences on advances in material technology for fossils power plants (2007) Page 371 – 387*

xxxiv. *Dionisio Laverde, Tomas Gomez-Acebo, Francisco Castro, Continuous and cyclic oxidation of T91 ferritic steel under steam, Corrosion Science 46 (2004) 613–631.*

xxxv. *A.P. Greeff, C.W. Louw, H.C. Swart, The oxidation of industrial FeCrMo steel, Corros. Sci. 42 (10) (2000) 1725.*

xxxvi. *J. Purbolaksono, A. Khinani, A.Z. Rashid, A.A. Ali, N.F. Nordin, Prediction of oxide scale growth in superheater and reheater tubes, Corrosion Science 51 (2009) 1022–1029,*

xxxvii. *I.G. Wright, R.B. Dooley, A review of the oxidation behaviour of structuralalloys in steam, Int. Mater. Rev. 55 (2010) 129–167.*

xxxviii. *Pantip Ampornrat *, Gary S. Was. Oxidation of ferritic–martensitic alloys T91, HCM12A and HT-9 in supercritical water, Journal of Nuclear Materials 371 (2007) 1–17.*

xxxix. *Juntao Yuana, Wen Wangb, Huihui Zhangb, Lijuan Zhua,b, Shenglong Zhub,Fuhui Wang, Investigation into the failure mechanism of chromia scale thermally grown on an austenitic stainless steel in pure steam, Corrosion Science (2016)*

xl. *A.P. Gree€, C.W. Louw, H.C. Swart*, The oxidation of industrial FeCrMo steel, Corrosion Science 42 (2000) Page 1725-1740.*